HAL
open science

Nanomechanical damping via electron-assisted relaxation of two-level systems

Olivier Maillet, Dylan Cattiaux, Xin Zhou, Rasul R. Gazizulin, Olivier Bourgeois, Andrew D. Fefferman, Eddy Collin

To cite this version:

Olivier Maillet, Dylan Cattiaux, Xin Zhou, Rasul R. Gazizulin, Olivier Bourgeois, et al.. Nanomechanical damping via electron-assisted relaxation of two-level systems. Physical Review B, 2023, 107 (6), pp.064104. 10.1103/PhysRevB.107.064104 . hal-03007076

HAL Id: hal-03007076

https://hal.science/hal-03007076v1

Submitted on 11 Jul 2023

HAL is a multi-disciplinary open access archive for the deposit and dissemination of scientific research documents, whether they are published or not. The documents may come from teaching and research institutions in France or abroad, or from public or private research centers.

L'archive ouverte pluridisciplinaire **HAL**, est destinée au dépôt et à la diffusion de documents scientifiques de niveau recherche, publiés ou non, émanant des établissements d'enseignement et de recherche français ou étrangers, des laboratoires publics ou privés.

Nanomechanical damping via electron-assisted relaxation of two-level systems

Olivier Maillet,[1,2,*] Dylan Cattiaux,[1] Xin Zhou,[1,3] Rasul R. Gazizulin,[1] Olivier Bourgeois,[1] Andrew D. Fefferman,[1] and Eddy Collin[1]

[1]*Université Grenoble Alpes, CNRS, Institut Néel, 38000 Grenoble, France*
[2]*Université Paris-Saclay, CEA, CNRS, SPEC, 91191 Gif-sur-Yvette Cedex, France*
[3]*CNRS, Université Lille, Centrale Lille, Université Polytechnique Hauts-de-France, IEMN UMR8520, Av. Henri Poincaré, Villeneuve d'Ascq 59650, France*

(Received 8 September 2020; accepted 6 February 2023; published 22 February 2023)

We report on measurements of dissipation and frequency noise at millikelvin temperatures of nanomechanical devices covered with aluminum. A clear excess damping is observed after switching the metallic layer from superconducting to the normal state with a magnetic field. Beyond the standard model of internal tunneling systems coupled to the phonon bath, here we consider the relaxation to the conduction electrons together with the nature of the mechanical dispersion laws for stressed/unstressed devices. With these key ingredients, a model describing the relaxation of two-level systems inside the structure due to interactions with electrons and phonons with well-separated timescales captures the data. In addition, we measure an excess $1/f$-type frequency noise in the normal state, which further emphasizes the impact of conduction electrons.

DOI: 10.1103/PhysRevB.107.064104

I. INTRODUCTION

Nanoelectromechanical systems (NEMS) [1] are now common tools used for ultra-sensitive detection [2] while being ubiquitous model systems for the study of quantum foundations involving mechanical degrees of freedom [3,4]. Both endeavours require resonators with high quality factors Q [5], so as to resolve either small frequency changes due to, e.g., masses added [2], or to preserve quantum coherence over long-enough times [6]. Yet mechanisms limiting the intrinsic Q factor of nanomechanical systems mostly remain a puzzle despite intensive efforts [7–9], especially at low temperature where quantum effects are expected to manifest themselves. Commonly proposed mechanisms include clamping losses [10] and higher-order phonon processes [11], e.g., thermoelastic damping [12] and Akhiezer damping [13]. While clamping losses are vanishingly small for thin beam structures [10], phonon-phonon interactions are switched off at low temperatures. In most cases, the surviving mechanism is thought to be the coupling between the mechanical strain arising from the resonator's motion and low-energy excitations in the constitutive material [7,9,14,15]. The excitations are either defects or (groups of) atoms that tunnel quantum mechanically between two nearly equivalent positions in the atomic lattice, hence forming two-level systems (TLS). These TLS cause damping of the mechanical motion through their interaction with the induced strain field and their own energy relaxation. The initial microscopic description of such a mechanism, the so-called standard tunneling model (STM), was introduced in the early 1970s [16,17] to explain low-temperature properties of amorphous materials and is still widely used nowadays, its importance being renewed by, e.g., superconducting circuits [18–21] or nanomechanics studies [9,14,15,22]. However, in the latter case, the model was unsuccessful in describing nanosystems which integrate resistive metallic elements [7,14,23].

In this article, we report the measurements from 10 K down to 30 mK of the damping rate and frequency shift of a high Q, high stress silicon nitride NEMS beam, covered with a thin aluminum layer (Fig. 1). Using different magnetic fields we can tune the metallic layer state from superconducting to normal below 1 K, revealing the unambiguous contribution to nanomechanical damping of the normal-state electrons reported for low-stress nanocantilevers [23]. To explain this contribution, we quantitatively include a mechanism of TLS relaxation due to the conduction electron bath [24] in parallel with phonon-assisted relaxation for a given fraction of the TLS distribution. The reasoning is formally equivalent to the one proposed in Ref. [8] where the authors introduced *ad hoc* a retarded (imaginary in frequency domain) Young's modulus whose microscopic origin is addressed in our work. The data are fit in all regimes, with a minimal set of free parameters. For comparison, the model also successfully reproduces the nanocantilever data of Ref. [23]. Details on the calculations and additional data can be found in the Supplementary Material (see Ref. [25] and references [26–28] therein). In addition, we measure the frequency noise as a function of temperature in both the normal and superconducting states. The magnitude is found to differ substantially between the two states, pointing again towards an electron-assisted mechanism. The results together with the model provide an answer to the issue of nanoelectromechanical damping in (hybrid) metallic systems at low temperatures, consistent with all the related results reported in the literature so far.

*olivier.maillet@cea.fr

 ©2023 American Physical Society

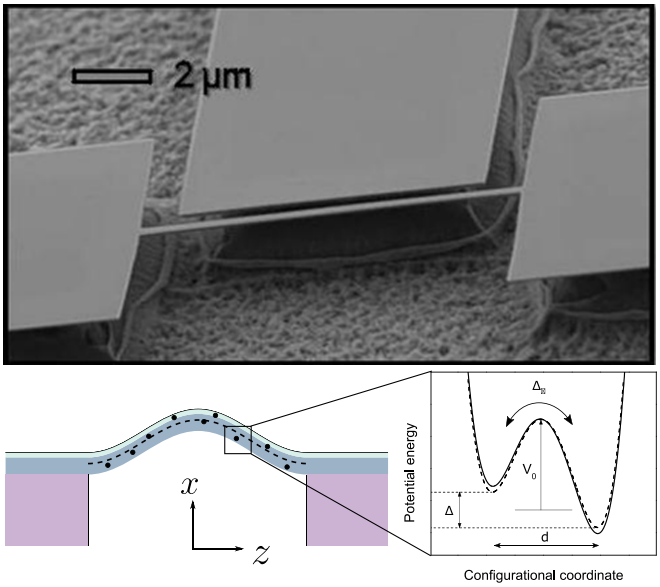

FIG. 1. Top: Scanning electron micrograph of the device (side gate electrode not used). Bottom: Schematic side view of NEMS (left) and TLS-strain coupling (right) under a macroscopic applied force. Right panel: Schematic potential energy of a single TLS at equilibrium (dashed) and under strain (full line). The two minima (separated by an energy gap Δ) are coupled through a tunneling element $\Delta_0 \propto e^{-d\sqrt{2m_a V_0}/\hbar}$, where V_0 is the barrier height, d the interwell distance, and m_a the tunneling entity effective mass.

II. EXPERIMENTAL RESULTS

The main sample is a 15-µm-long silicon nitride beam covered with 30-nm aluminum, having transverse dimensions $e \times w = 130\,\text{nm} \times 300\,\text{nm}$ (see Fig. 1) and mounted on a cold finger thermally anchored to the mixing chamber stage of a dilution refrigerator in cryogenic vacuum. The motion of the fundamental out-of-plane flexural mode of the beam at a frequency $\omega = 2\pi \times 17.5$ MHz is actuated and detected with the magnetomotive scheme [29], the electromotive signal being detected by a lock-in amplifier [see Fig. 2(a)]. The Al layer (whose critical temperature at zero magnetic field is measured to be $T \approx 1.4$ K) is quenched at all temperatures for in-plane magnetic fields larger than 320 mT, and all the data in the normal state are obtained for fields larger than 600 mT. Damping and frequency shift due to remaining magnetomotive losses [29] or to intermediate superconducting properties [23] are carefully characterized and subtracted to reveal the intrinsic mechanical damping. For each measurement point in the normal state, we used low excitation currents to minimize Joule heating. The measurements were repeated over several thermal cycles and found reproducible.

We observe a logarithmic dependence of the frequency shift $\delta\omega_0/\omega_0 = C\ln(T/T_0)$ [with respect to an arbitrary reference ω_0, see Fig. 2(b)] below 1 K, which we interpret as evidence for TLS-driven behavior [17], in particular since $C = 2.1 \times 10^{-5}$ agrees with the commonly reported values for similar structures [7,9,14]. This behavior arises from the resonant interaction of applied phonons through magnetomotive driving and TLSs [17] (while the relaxational interaction, which we address further in this work to interpret the damping measurements, yields a T^6 dependence at low temperature [30], which is negligible compared to the resonant contribution to the frequency shift). The frequency shift above 1 K follows a T^3 law which we attribute to thermal expansion mismatch between the two layers [31]. Meanwhile, the measured damping rate represented in Fig. 3 is divided into two regimes in temperature: above 1 to 2 K it essentially reaches a nearly constant plateau around 1.2 kHz. Below 600 mK at low magnetic field (metallic layer in the superconducting state), it decreases linearly with temperature. Below typically 70 mK, the damping rate and frequency shift measurements were rendered complicated by both frequency noise (which is no longer negligible compared to the typical damping rate) and by the low signals measured as a result of a low (<100 mT) magnetic field application. This explains why the dispersion on the data and the error bars are significant at 30 mK.

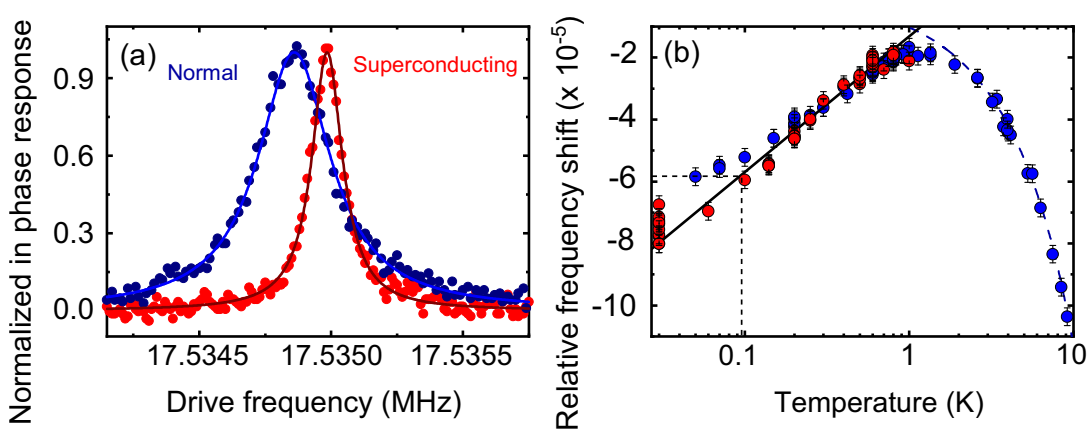

FIG. 2. (a) NEMS in-phase response to a small magnetomotive excitation at $T = 275$ mK in superconducting (red dots) and normal (blue dots) states of the metallic layer, normalized to their peak height for better comparison. Solid lines are Lorentzian fits. The resonance frequency difference is due to the magnetomotive contribution and the magnetomotive damping contribution accounts for 5% of the line width in the normal state. (b) Relative frequency shift $\delta\omega_0/\omega_0$ as a function of refrigerator's base temperature. The line is a logarithmic fit, while the dashed blue curve is a T^3 empirical law (see text). The dotted line indicates that, by using the frequency shift as a thermometer, the electron temperature could be about 100 mK when the cryostat's base temperature is 50 mK (see text).

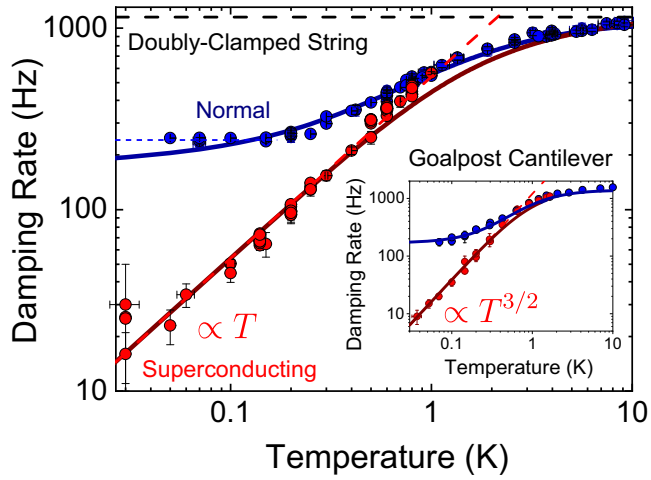

FIG. 3. NEMS damping rate as a function of refrigerator's base temperature in normal (blue) and superconducting (red) states, with the magnetomotive contribution subtracted. Inset: Data from Ref. [23]. Solid curves (main and inset) are fits using Eq. (2) with relaxation rates due to phonons [Eq. (3)] and electrons [Eq. (4)] to electrons. Dashed red and black lines correspond to low- and high-temperature asymptotic behaviors, respectively. The blue dotted line indicates a possible saturation above 100 mK due to thermal decoupling (see text).

Switching the metallic layer to the normal state with the magnetic field leads to a strikingly different dissipation rate (see Fig. 3, blue dots) below 700–800 mK, while it does not contribute further to the resonance frequency shift within our experimental accuracy [see Fig. 2(b)] down to roughly 200 mK. Below this temperature, the frequency shift in the normal state slightly deviates from the logarithmic trend. Those observations complement previous results [23] obtained with a low-stress goalpost-shaped silicon nanoresonator (see Fig. 3, inset), with very similar features. This suggests that the mechanism at stake in the normal state is independent of geometry or mechanical properties. Between roughly 150 mK and 1 K the damping in the normal state shows a sublinear power-law-like behavior and reaches a saturation threshold for lower temperatures, consistently with previous measurements in similar conditions [7,14,32] where T^{α}, $\alpha = 0.3$–0.7 dependences were reported. Note that the saturation temperature range roughly coincides with the range where the frequency shift deviates from the logarithmic trend. We ascertain that the extra damping in the normal state, down to 50 mK, is not caused by a mechanical nonlinearity: the damping rate remains unaffected by the displacement amplitude within our experimental accuracy [25]. Additionally, it does not depend on the current levels injected [25] in our experimental range (up to ~ 70 nA), consistently with Ref. [23]. This rules out Joule dissipation due to the driving scheme as a mechanism of damping saturation as well as a significant cause of thermal decoupling.

III. INTERPRETATION IN THE SUPERCONDUCTING STATE

The temperature dependence in the superconducting state can be explained using the canonical STM appended with NEMS constraints such as low-dimensionality [15,33]. In addition, the high tensile stress is shown to quantitatively affect the magnitude of TLS-induced damping [25,34] (but not the NEMS elastic constants). Let us consider a TLS inside the structure with asymmetry Δ and tunneling amplitude Δ_0 between the two potential wells (see Fig. 1). Considering only the local ground state of each well (the first excited state of energy comparable with Debye energy, is irrelevant at low temperatures), the bare Hamiltonian of a single TLS is analogous to that of a 1/2 spin. It writes in the TLS position basis corresponding to left and right well locations: $\mathcal{H}_0 = 1/2(\Delta_0\hat{\sigma}_x + \Delta\hat{\sigma}_z)$, where $\hat{\sigma}_{x,z}$ are Pauli matrices. The TLS eigenstates energies are then easily obtained $\varepsilon_{\pm} = \pm 1/2\sqrt{\Delta^2 + \Delta_0^2}$, with corresponding wave functions that are delocalized over the two wells. Following the usual STM framework, the NEMS is put into an oscillating motion at angular frequency ω and the structure undergoes an axial oscillating strain $\mathcal{E}$. The strain field changes the local potential energy landscape that defines the TLS, leading to a modulation of its energy splitting $\varepsilon = \sqrt{\Delta^2 + \Delta_0^2}$, formalized by the coupling Hamiltonian in the TLS position basis $\hat{\mathcal{H}}_{\text{int}} = \gamma\mathcal{E}\hat{\sigma}_z$, with $\gamma = \frac{1}{2}\partial\Delta/\partial\mathcal{E}$ the TLS-strain coupling strength and $\hat{\sigma}_z$ the TLS diagonal Pauli matrix. Subsequently, the TLS returns to equilibrium by exchanging energy with the phonon bath (the thermal strain field) following the same coupling Hamiltonian over a characteristic time τ. This causes a lagging stress response, leading to mechanical energy dissipation. The power dissipated per unit volume V is written as

$$P_V = \frac{P_0\omega(\gamma\mathcal{E}_0)^2}{2}\int_0^{\infty} du \int_0^1 dv \frac{v^2}{1-v^2}\,\text{sech}^2\left(\frac{u}{2}\right) \times \frac{\omega\tau(u,v,T)}{1+\omega^2\tau^2(u,v,T)}, \tag{1}$$

with $\mathcal{E}_0$ the strain oscillation amplitude and P_0 the TLS density of states per unit volume. For a string undergoing flexure [11], the macroscopic-imposed strain field oscillates with an amplitude $\mathcal{E}_0 \propto \frac{\partial^2\Psi(z)}{\partial z^2}x_0$, where x_0 is the NEMS oscillation amplitude at mid abscissa and $\Psi(z)$ is the excited mode shape. For a high-stress doubly clamped beam, the fundamental flexural mode shape writes: $\Psi(z) = \cos(\pi z/l)$ with $z = 0$ at midabscissa of the beam. The total power P is first obtained through integration of P_V in Eq. (1) over the NEMS dimensions [25]. It is then independently obtained by macroscopic arguments, using the mode dynamics equation: $P = \frac{1}{2}m\omega^2x_0^2\Gamma$, where $m = \rho ew\int\Psi^2(z)dz = \rho ewl/2$ is the effective mass of the NEMS in its fundamental out-of-plane flexural mode, with ρ being its mass density. By equating the two expressions, we thus obtain the generic expression of the TLS ensemble contribution to the NEMS damping rate resulting from the strain modulation [25]

$$\Gamma[\tau] = C\omega\iint d\varepsilon d\Delta P(\varepsilon,\Delta)\left(\frac{\Delta}{\varepsilon}\right)^2\text{sech}^2\left(\frac{\varepsilon}{2k_BT}\right) \times \frac{\omega\tau(\varepsilon,\Delta)}{1+\omega^2\tau^2(\varepsilon,\Delta)}. \tag{2}$$

Here we introduce the commonly assumed [17] TLS distribution $P(\varepsilon,\Delta) = \varepsilon/(\varepsilon^2 - \Delta^2)$ and $C = P_0\gamma^2\pi^2e^2/12\sigma_0l^2$, with $\sigma_0 = 1.1 \pm 0.1$ GPa the in-built axial stress. Note that C is the-

oretically identical to the logarithmic slope of the frequency shift [35], but its expression differs from the one commonly derived [35] due to the influence of high tensile stress on the excited flexural mode [25]. For high-enough temperatures, the damping reaches a plateau $\pi\omega C/2$, regardless of microscopic TLS scattering mechanisms. From the measured plateau we extract $C = 4.3 \times 10^{-5}$, in qualitative agreement but differing by a factor of 2 from the value given by the frequency shift measurement. Similar discrepancies were reported [7,9,14,23] and may be due to our simplified model that neglects, e.g., the bilayer structure or inhomogeneities in the TLS distribution.

Below 600 mK, the measured linear dependence is consistent with previous reports for similar beams [9,36], but is in contradiction with the usual T^3 dependence. However, at subkelvin temperatures, the dominant phonon wavelength $\lambda = hc/2.82k_BT$ ($\sim$100 nm at 1 K) becomes bigger than the transverse dimensions of the resonator. As a result TLS relax to equilibrium by exchanging energy only with longitudinal phonon modes [25], which are not confined and thus lie at lower energies. They realize a quasi-one-dimensional phonon bath with constant density of states $l/\pi c_l$ and linear dispersion relation, as proposed, e.g., in Refs. [9,36] and more extensively studied in Refs. [15,33,34]. At first nonvanishing order in the thermal strain field perturbation, Fermi's Golden Rule yields the relaxation rate of a single TLS due to its interaction with the phonon bath [15,25]

$$\tau_{ph}^{-1} = \frac{\gamma^2}{\hbar^2 \rho e w c_l^3} \frac{\Delta_0^2}{\varepsilon} \coth\left(\frac{\varepsilon}{2k_BT}\right), \tag{3}$$

where $c_l \sim 6000$ m/s and $\rho = 2.9 \times 10^3$ kg/m^3 are the longitudinal sound speed and mass density for SiN, respectively. Combining this relaxation rate with the damping expression (2), we capture both the damping data in the low-temperature range when the field is low enough to maintain superconductivity in the metallic layer and the high-temperature limit. To consistently fit both the low ($\Gamma[\tau_{ph}] \propto \gamma^2 CT$, dashed red line in Fig. 3) and high ($\Gamma[\tau_{ph}] \propto C$) temperature regimes we use $\gamma = 9.8$ eV and $P_0 = 2.2 \times 10^{44}$ J^{-1} m^{-3}. The fitted interaction energy is rather high (one would expect it more around 1 eV), but may likely reflect a nonuniform distribution of the TLS inside the beam [22], which is out of the scope of this study. Note that our expression does not fit the data in the superconducting state between 600 mK and 1 K, which we attribute to the substantial density of quasiparticle excitations in this range, that should contribute to an excess damping through the same mechanism as electrons in the normal state [37]: in fact, above 800 mK the data in both states are identical within experimental accuracy, as observed previously [23]. This shall be addressed elsewhere.

IV. INTERPRETATION IN THE NORMAL STATE

In the normal state, it is natural to consider the conduction electrons as an additional relaxation channel for TLS in parallel with the phonon bath: when a TLS entity tunnels, the Coulomb potential that scatters conduction electrons is modified, which translates as an effective electron-TLS coupling. The effective Hamiltonian writes $\mathcal{H}_{el} = \sum V_{k,k'} \hat{c}_{k'}^{\dagger} \hat{c}_k \hat{\sigma}_z$, where $\hat{\sigma}_z$ is the TLS diagonal Pauli matrix, $\hat{c}_k^{(\dagger)}$ the electron creation (annihilation) operator at wave vector k and $V_{k,k'}$ the coupling matrix elements. We further make the assumption that the interaction is uniform near the surface of the Fermi sea, which enables the simplification $V_{k,k'} \approx V$. This is reasonable insofar as electronic excitations are scattered within a bandwidth k_BT very small compared to the Fermi energy. The corresponding relaxation rate is again obtained by Fermi's Golden Rule [25]

$$\tau_{el}^{-1} = \frac{4\pi K}{\hbar} \frac{\Delta_0^2}{\varepsilon} \coth\left(\frac{\varepsilon}{2k_BT}\right), \tag{4}$$

where $K = (n_0 V \Omega)^2$ is a normalized electron-TLS coupling strength, $n_0 = 1.07 \times 10^{47}$ J^{-1}m^{-3} being the electronic density of states at the Fermi level for aluminum, V an averaged coupling constant, and Ω the effective interaction volume, which should vanish beyond the metallic screening length ($\lesssim$1 nm). The energy dependence is the same as in the case of phonon-assisted relaxation, which led previous studies to invoke additional effects [7]. However, the averaging over the full TLS distribution leads to a weakened dependence in temperature of the damping rate in the normal state. Indeed, it is certain that not all TLS interact with electrons due not only to the fact that conduction electrons are located solely in the metallic layer, but also because of the very nature of the TLS-electron interaction: depending on the microscopic nature of the TLS, the interaction may be very weak, as in the case of a mere dislocation in the Al layer [9]. Therefore, electrically "neutral" TLS interact with phonons, but not with electrons, which leads to separate averages over charged and neutral TLS.

For "neutral" TLS and TLS within the SiN layer, which relax only due to interactions with phonons, the crossover temperature T_{ph}^* between the plateau and the power-law regime is defined by the condition $\omega\tau_{ph} \sim 1$ that they must all satisfy. Meanwhile, for charged TLS, the crossover temperature T_{el}^* is shifted down by electron-assisted relaxation because for these TLS the condition $\omega\tau \sim 1$, where now $\tau^{-1} = \tau_{ph}^{-1} + \tau_{el}^{-1}$, is modified. Thus, for $T_{el}^* < T < T_{ph}^*$, an intermediate regime emerges. At ultra-low temperatures, the $\propto T$ relaxation regime should be recovered when all TLS in the structure satisfy $\omega\tau \gg 1$. We fit the data in the normal state using a balanced expression of the damping rate $\Gamma_N = (1-x)\Gamma[\tau_{ph}] + x\Gamma[(\tau_{ph}^{-1} + \tau_{el}^{-1})^{-1}]$ using for the two contributions the generic form of Eq. (2), by assuming a fraction $x = 0.17$ of TLS interacting with electrons with a coupling constant $K = 0.07$ well below 1, which allows us to neglect Kondo-type strong coupling corrections [38,39], yielding an electron-TLS coupling energy V in the 0.1-eV range. Based on this set of parameters, we evaluate crossover temperatures $T_{ph}^* \approx 1$ K (as visible in Fig. 3) and $T_{el}^* \approx 0.9$ mK [25], the latter being unreachable with standard dilution refrigeration. For comparison, we have also fit the data obtained on another sample, namely, the goalpost-shaped silicon nanocantilever (with dimensions comparable to the SiN beam, 100-nm thick $\times$ 250-nm wide, two 3-μm long feet linked by a 7-μm long paddle), covered with a 50-nm aluminum layer similar to that of the high-stress SiN sample, measured in Ref. [23]. The dissipation in the superconducting state features a $T^{3/2}$

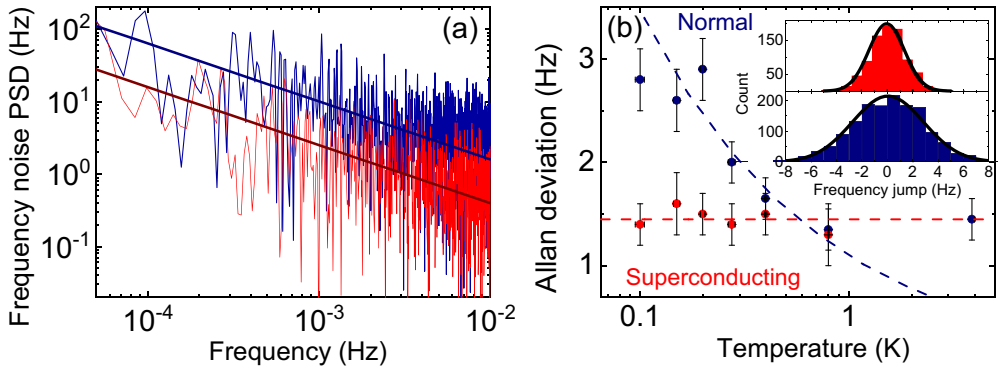

FIG. 4. (a) Frequency noise spectrum at $T = 100$ mK in the superconducting (red) and normal (blue) state of the metallic layer. Solid lines are $1/f^{\mu}$ type functions, with $\mu = 0.8 \pm 0.2$ here. (b) Allan deviation $\sqrt{\langle \delta f^2 \rangle}$ of frequency noise (δf is the jump between two successive frequency measurements), extracted from the standard deviation of Gaussian fits to the jumps histograms. Dashed lines (constant for the superconducting state, $\propto 1/\sqrt{T}$ for the normal state) are guides to the eye. Inset: Comparison of frequency jumps histograms in the superconducting and normal state at $T = 100$ mK. Solid lines are Gaussian fits with mean $\langle \delta f \rangle = 0$ and standard deviation thus directly reflecting the Allan deviation measured over $\sim 10^4$ s.

power law at low temperatures which might owe to a nonlinear dispersion relation of flexural mechanical modes in the device [40]. The data are reproduced using a semi-phenomenological expression for the TLS-phonon relaxation rate [25]. The normal state data were fit with parameters $x = 0.12$ and $K = 0.11$, comparable with the ones used for the high stress SiN sample. This is consistent with a mechanism independent from the mechanical properties of the resonator, as the interaction lengthscale is much smaller than any mechanical dimension.

The model captures the data in the 0.15 to 1 K range, as seen in Fig. 3. In particular, it reproduces the sublinear power-law-like behavior consistently reported in previous works [7,14,23] in similar experimental conditions. Although our model captures to a large extent the saturation observed below 150 mK and reported in nearly every nanomechanical damping study for the lowest operation temperatures, it is likely that a hot electron effect also causes overheating of the structure [41]. This saturation can be estimated through the frequency shift measured in the normal state: it provides a thermometer by using the deviation from the logarithmic shift at the lowest temperatures. This could mean that the electron temperature does not go lower than 100 mK at the lowest refrigerator temperature (50 mK) in the normal state [see Fig. 2(b), blue dots]. This is consistent, within experimental accuracy, with the observed damping saturation slightly above the theoretical fit below 100 mK (see Fig. 3, blue dotted line). We could attribute these two features to thermal decoupling caused by parasitic radiation in the 10 pW range, which heats up the aluminum layer, i.e., the electron bath to which the TLS ensemble (and ultimately, then, the mechanical mode) thermalize [25]. Ultimately, we see evidence, supported by our analysis, that both thermal decoupling and the TLS-induced damping contribute to the damping saturation in the normal state at the lowest operation temperatures, but more work is needed to separate the two contributions.

The proposed modeling is fairly generic and makes minimal assumptions on the microscopic nature and location of TLS. An educated guess based on our results would locate those TLS which interact with electrons at the interfaces, between the SiN and Al layer, and between the Al layer and its native oxide at the NEMS surface: indeed, tunneling atoms are less likely to exist within the metallic layer due to long-range order, leaving kinks on dislocations, which are only weakly interacting with electrons, as most probable candidates for TLS in polycrystalline aluminum, as proposed in Refs. [9,30].

Note that a recent study with similar methods [42] but bare aluminum resonators reports very little difference between damping in the normal and superconducting state, with a much smaller interaction constant $V \sim 10^{-4}$ eV. This may be seen as further evidence that aluminum does not itself possess defects that would act as strongly interacting TLS and also points towards a location of interacting TLS at the Al-SiN interface rather than in the Al native oxide.

As an opening for further investigations, we measured the resonant frequency noise of our device using the dynamical bifurcation properties of the NEMS in the Duffing regime [43,44]. The observed spectrum is that of a $1/f$-type noise typical of a collection of switching two-level systems [45]. Notably, a visible increase of its magnitude is observed below 1 K when the metallic layer is switched to the normal state, as seen in Fig. 4. Since at these temperatures the switching, which is due to tunneling, is mainly induced by TLS-electrons interactions, it is reasonable to expect that electron-TLS interactions cause the excess frequency noise: the tunneling events occurring during TLS relaxation cause local rearrangement of atoms and may thus lead to stress (i.e., frequency) fluctuations.

In conclusion, our results support the idea that electron-driven TLS relaxation in metallic nanomechanical structures is the dominant mechanism of damping, through timescale decoupling between phonon- and electron-induced TLS relaxation. This may bring an answer to several issues raised over the last two decades by nanomechanical damping measurements at low temperatures. In addition, we expect that measurements of frequency noise may shed further light on microscopic mechanisms at work, possibly highlighting interactions between TLS [46], through, e.g., a careful extraction of the exponent of frequency noise [47].

ACKNOWLEDGMENTS

We acknowledge the use of the Néel facility *Nanofab* for the device fabrication. We acknowledge support from the ERC CoG Grant No. ULT-NEMS 647917, StG Grant No. UNIGLASS 714692. The research leading to these results received funding from the European Union's Horizon 2020 Research and Innovation Programme, under Grant Agreement No. 824109, the European Microkelvin Platform (EMP).

[1] H. G. Craighead, Nanoelectromechanical systems, Science **290**, 1532 (2000).

[2] J. Chaste, A. Eichler, J. Moser, G. Ceballos, R. Rurali, and A. Bachtold, A nanomechanical mass sensor with yoctogram resolution, Nat. Nanotechnol. **7**, 301 (2012).

[3] A. D. O'Connell, M. Hofheinz, M. Ansmann, R. C. Bialczak, M. Lenander, E. Lucero, M. Neeley, D. Sank, H. Wang, M. Weides, J. Wenner, J. M. Martinis, and A. N. Cleland, Quantum ground state and single-phonon control of a mechanical resonator, Nature (London) **464**, 697 (2010).

[4] C. F. Ockeloen-Korppi, E. Damskägg, J.-M. Pirkkalainen, M. Asjad, A. A. Clerk, F. Massel, M. J. Woolley, and M. A. Sillanpää, Stabilized entanglement of massive mechanical oscillators, Nature (London) **556**, 478 (2018).

[5] A. H. Ghadimi, S. A. Fedorov, N. J. Engelsen, M. J. Bereyhi, R. Schilling, D. J. Wilson, and T. J. Kippenberg, Elastic strain engineering for ultralow mechanical dissipation, Science **360**, 764 (2018).

[6] D. J. Wilson, V. Sudhir, N. Piro, R. Schilling, A. Ghadimi, and T. J. Kippenberg, Measurement-based control of a mechanical oscillator at its thermal decoherence rate, Nature (London) **524**, 325 (2015).

[7] G. Zolfagharkhani, A. Gaidarzhy, S.-B. Shim, R. L. Badzey, and P. Mohanty, Quantum friction in nanomechanical oscillators at millikelvin temperatures, Phys. Rev. B **72**, 224101 (2005).

[8] Q. P. Unterreithmeier, T. Faust, and J. P. Kotthaus, Damping of Nanomechanical Resonators, Phys. Rev. Lett. **105**, 027205 (2010).

[9] F. Hoehne, Y. A. Pashkin, O. Astafiev, L. Faoro, L. B. Ioffe, Y. Nakamura, and J. S. Tsai, Damping in high-frequency metallic nanomechanical resonators, Phys. Rev. B **81**, 184112 (2010).

[10] I. Wilson-Rae, Intrinsic dissipation in nanomechanical resonators due to phonon tunneling, Phys. Rev. B **77**, 245418 (2008).

[11] A. N. Cleland, *Foundations of Nanomechanics*, 2003rd ed. (Springer, Berlin, 2002).

[12] R. Lifshitz and M. L. Roukes, Thermoelastic damping in micro- and nanomechanical systems, Phys. Rev. B **61**, 5600 (2000).

[13] S. S. Iyer and R. N. Candler, Mode- and Direction-Dependent Mechanical Energy Dissipation in Single-Crystal Resonators due to Anharmonic Phonon-Phonon Scattering, Phys. Rev. Appl. **5**, 034002 (2016).

[14] A. Venkatesan, K. J. Lulla, M. J. Patton, A. D. Armour, C. J. Mellor, and J. R. Owers-Bradley, Dissipation due to tunneling two-level systems in gold nanomechanical resonators, Phys. Rev. B **81**, 073410 (2010).

[15] B. D. Hauer, P. H. Kim, C. Doolin, F. Souris, and J. P. Davis, Two-level system damping in a quasi-one-dimensional optomechanical resonator, Phys. Rev. B **98**, 214303 (2018).

[16] P. W. Anderson, B. I. Halperin, and C. M. Varma, Anomalous low-temperature thermal properties of glasses and spin glasses, Philos. Mag. **25**, 1 (1972).

[17] W. A. Phillips, Tunneling states in amorphous solids, J. Low Temp. Phys. **7**, 351 (1972).

[18] J. M. Martinis, K. B. Cooper, R. McDermott, M. Steffen, M. Ansmann, K. D. Osborn, K. Cicak, S. Oh, D. P. Pappas, R. W. Simmonds, and C. C. Yu, Decoherence in Josephson Qubits from Dielectric Loss, Phys. Rev. Lett. **95**, 210503 (2005).

[19] T. Capelle, E. Flurin, E. Ivanov, J. Palomo, M. Rosticher, S. Chua, T. Briant, P.-F. Cohadon, A. Heidmann, T. Jacqmin, and S. Deléglise, Probing a Two-Level System Bath via the Frequency Shift of an Off-Resonantly Driven Cavity, Phys. Rev. Appl. **13**, 034022 (2020).

[20] C. Müller, J. H. Cole, and J. Lisenfeld, Towards understanding two-level-systems in amorphous solids: Insights from quantum circuits, Rep. Prog. Phys. **82**, 124501 (2019).

[21] H. le Sueur, A. Svilans, N. Bourlet, A. Murani, L. Bergé, L. Dumoulin, and P. Joyez, Microscopic charged fluctuators as a limit to the coherence of disordered superconductor devices, arXiv:1810.12801.

[22] M. Hamoumi, P. E. Allain, W. Hease, E. Gil-Santos, L. Morgenroth, B. Gérard, A. Lemaître, G. Leo, and I. Favero, Microscopic Nanomechanical Dissipation in Gallium Arsenide Resonators, Phys. Rev. Lett. **120**, 223601 (2018).

[23] K. J. Lulla, M. Defoort, C. Blanc, O. Bourgeois, and E. Collin, Evidence for the Role of Normal-State Electrons in Nanoelectromechanical Damping Mechanisms at Very Low Temperatures, Phys. Rev. Lett. **110**, 177206 (2013).

[24] S. Hunklinger and A. K. Raychaudhuri, Thermal and elastic anomalies in glasses at low temperatures, in *Progress in Low Temperature Physics*, Vol. 9, edited by D. F. Brewer, (Elsevier, New York, 1986), Chap. 3, pp. 265–344.

[25] See Supplemental Material at http://link.aps.org/supplemental/10.1103/PhysRevB.107.064104 for details on the calculations and additional data and the references therein.

[26] R. O. Pohl, X. Liu, and E. Thompson, Low-temperature thermal conductivity and acoustic attenuation in amorphous solids, Rev. Mod. Phys. **74**, 991 (2002).

[27] J. D. Teufel, J. W. Harlow, C. A. Regal, and K. W. Lehnert, Dynamical Backaction of Microwave Fields on a Nanomechanical Oscillator, Phys. Rev. Lett. **101**, 197203 (2008).

[28] X. Zhou, D. Cattiaux, R. R. Gazizulin, A. Luck, O. Maillet, T. Crozes, J.-F. Motte, O. Bourgeois, A. Fefferman, and E. Collin, On-chip Thermometry for Microwave Optomechanics Implemented in a Nuclear Demagnetization Cryostat, Phys. Rev. Appl. **12**, 044066 (2019).

[29] A. N. Cleland and M. L. Roukes, External control of dissipation in a nanometer-scale radiofrequency mechanical resonator, Sens. Actuators A: Phys. **72**, 256 (1999).

[30] A. D. Fefferman, R. O. Pohl, and J. M. Parpia, Elastic properties of polycrystalline Al and Ag films down to 6 mK, Phys. Rev. B **82**, 064302 (2010).

[31] E. Collin, J. Kofler, S. Lakhloufi, S. Pairis, Y. M. Bunkov, and H. Godfrin, Metallic coatings of microelectromechanical structures at low temperatures: Stress, elasticity, and nonlinear dissipation, J. Appl. Phys. **107**, 114905 (2010).

[32] M. Imboden and P. Mohanty, Evidence of universality in the dynamical response of micromechanical diamond resonators at millikelvin temperatures, Phys. Rev. B **79**, 125424 (2009).

[33] R. O. Behunin, F. Intravaia, and P. T. Rakich, Dimensional transformation of defect-induced noise, dissipation, and nonlinearity, Phys. Rev. B **93**, 224110 (2016).

[34] O. Maillet, Stochastic and Non-Linear Processes in nano-electro-mechanical systems, Theses, Université Grenoble Alpes (2018).

[35] W. A. Phillips, Two-level states in glasses, Rep. Prog. Phys. **50**, 1657 (1987).

[36] J. Sulkko, M. A. Sillanpää, P. Häkkinen, L. Lechner, M. Helle, A. Fefferman, J. Parpia, and P. J. Hakonen, Strong gate coupling of high-q nanomechanical resonators, Nano Lett. **10**, 4884 (2010).

[37] O. Suchoi and E. Buks, Damping in a superconducting mechanical resonator, Europhys. Lett. **117**, 57008 (2017).

[38] S. N. Coppersmith and B. Golding, Low-temperature acoustic properties of metallic glasses, Phys. Rev. B **47**, 4922 (1993).

[39] A. J. Leggett, S. Chakravarty, A. T. Dorsey, M. P. A. Fisher, A. Garg, and W. Zwerger, Dynamics of the dissipative two-state system, Rev. Mod. Phys. **59**, 1 (1987).

[40] C. Seoánez, F. Guinea, and A. H. Castro Neto, Surface dissipation in nanoelectromechanical systems: Unified description with the standard tunneling model and effects of metallic electrodes, Phys. Rev. B **77**, 125107 (2008).

[41] M. L. Roukes, M. R. Freeman, R. S. Germain, R. C. Richardson, and M. B. Ketchen, Hot Electrons and Energy Transport in Metals at Millikelvin Temperatures, Phys. Rev. Lett. **55**, 422 (1985).

[42] T. Kamppinen, J. T. Mäkinen, and V. B. Eltsov, Dimensional control of tunneling two-level systems in nanoelectromechanical resonators, Phys. Rev. B **105**, 035409 (2022).

[43] J. S. Aldridge and A. N. Cleland, Noise-Enabled Precision Measurements of a Duffing Nanomechanical Resonator, Phys. Rev. Lett. **94**, 156403 (2005).

[44] O. Maillet, X. Zhou, R. R. Gazizulin, R. Ilic, J. M. Parpia, O. Bourgeois, A. D. Fefferman, and E. Collin, Measuring frequency fluctuations in nonlinear nanomechanical resonators, ACS Nano **12**, 5753 (2018).

[45] P. Dutta and P. M. Horn, Low-frequency fluctuations in solids: $1/f$ noise, Rev. Mod. Phys. **53**, 497 (1981).

[46] A. D. Fefferman, R. O. Pohl, A. T. Zehnder, and J. M. Parpia, Acoustic Properties of Amorphous Silica between 1 and 500 mK, Phys. Rev. Lett. **100**, 195501 (2008).

[47] L. Faoro and L. B. Ioffe, Interacting tunneling model for two-level systems in amorphous materials and its predictions for their dephasing and noise in superconducting microresonators, Phys. Rev. B **91**, 014201 (2015).